ADVANCED FUNCTIONAL MATERIALS
www.afm-journal.de

High Efficiency Solid-State Dye-Sensitized Solar Cells Assembled with Hierarchical Anatase Pine Tree-like TiO_2 Nanotubes

*Dong Kyu Roh, Won Seok Chi, Harim Jeon, Sang Jin Kim, and Jong Hak Kim**

A facile and effective method to prepare hierarchical pine tree-like TiO_2 nanotube (PTT) arrays with an anatase phase directly grown on a transparent conducting oxide substrate via a one-step hydrothermal reaction. The PTT arrays consist of a vertically oriented long nanotube (NT) stem and a large number of short nanorod (NR) branches. Various PTT morphologies are obtained by adjusting the water/diethylene glycol ratio. The diameter of the NTs and the size of the NR branches decreases from 300 to100 nm and from 430 to 230 nm, respectively, with increasing water content. The length of the PTT arrays could be increased up to 19 μm to significantly improve the charge transport and specific surface area. The solid-state dye-sensitized solar cells (ssDSSC) assembled with the 19 μm long PTT arrays exhibit an outstanding energy-conversion efficiency of 8.0% at 100 mW/cm^2, which is two-fold higher than that of commercially available paste (4.0%) and one of the highest values obtained for N719 dye-based ssDSSCs. The high performance is attributed to the larger surface area, improved electron transport, and reduced electrolyte/electrode interfacial resistance, resulting from the one-dimensional, well-aligned structure with a high porosity and large pores.

1. Introduction

Since the prototype of dye-sensitized solar cells (DSSCs) was developed by the Gratzel group in 1991, they have attracted a lot of attention as an alternative to silicon solar cells due to their high photoconversion efficiency, low cost, and facile fabrication process.[1] Despite the high energy conversion efficiency of DSSCs with a I^-/I_3^- liquid electrolyte,[2] solid-state DSSCs (ssDSSCs) have recently received much attention due to the need for long-term stability, flexible design, and lightweight cells.[3–8] Several approaches have been reported for ssDSSCs based on a hole conducting polymer[9–14] or a solid polymer electrolyte.[15–17] However, most of the reported efficiencies of ssDSSCs are less than 7%, which is less than the efficiencies of their counterparts using a liquid electrolyte.[3–17] Recently, the Kanatzidis group reported a high efficiency of 8.5% of a ssDSSC using a $CsSnI_3$ perovskite as a hole conductor.[18] High efficiencies of 10.9% and 9.7% were also independently reported by the Snaith and Park groups, respectively, using $(CH_3NH_3)PbX$ (X = Cl, I) perovskite and spiro-MeOTAD as a light harvester and a hole conductor, respectively.[19] However, these high efficiencies in ssDSSCs were all based on the development of a novel hole conductor or sensitizer, implying that the cell performance could be further improved if it is combined with the development of a more effective TiO_2 photoanode.

Typically, a nanocrystalline TiO_2 photoanode is fabricated with randomly-organized, disordered nanoparticles, which provides a large surface area for anchoring sufficient dye molecules, resulting in an increase of the current density. However, high charge recombination with I_3^- in the electrolyte due to the large grain boundary of nanoparticles and the random walk of photoinjected electrons through the nanoparticulate film may reduce the charge collection efficiency in DSSCs. Recently, well-aligned photoanodes have been fabricated based on nanorods (NRs),[20] nanowires (NWs),[21] nanotubes (NTs),[22] nanosheets,[23] and nanospheres[24] to improve the cell performance. In particular, vertically aligned one-dimensional (1D) nanostructured photoanodes such as NWs and NTs are considered to be ideal to promote charge transport because they provide a direct transport pathway for photoinjected electrons.[25] However, the low specific surface area of 1D-nanostructured photoanodes results in a limited low energy conversion efficiency due to insufficient dye loading and thus, a low current density.

One of the approaches to increase the surface area to improve cell performance is to increase the length of TiO_2 NWs or NTs. Energy conversion efficiencies of 2.87% for a 25 μm TiO_2 NW array film[26] and 4.82% for a 35 μm TiO_2 NT array film[27] were reported. Although enlarging the length increases the surface area for dye adsorption, the efficiency is still lower than 5% even in liquid-state DSSCs, indicating that there are some limitations to improve the cell performance by only enlarging the TiO_2 length. The extremely long length makes it difficult to transport charges because the photoinjected

D. K. Roh, W. S. Chi, H. Jeon, S. J. Kim, Prof. J. H. Kim
Department of Chemical and Biomolecular Engineering
Yonsei University, 262 Seongsanno
Seodaemun-gu, Seoul, 120–749, South Korea
E-mail: jonghak@yonsei.ac.kr

DOI: 10.1002/adfm.201301562

electrons have to travel a long distance and therefore, losses of electrons can easily occur through the photoanode. In particular, in ssDSSC applications, the pore-filtration of large molecular volume polymer electrolyte in such a thick film is less effective,[28] which increases the cell resistance leading to reduced cell performance. To overcome the drawback of a low specific surface area, dendritic NRs with a larger surface roughness and surface area were developed on the surface of NWs and NTs.[29] NWs or NTs surface-modified with dendritic NRs could improve both the specific surface area and charge transport properties, resulting in an improvement of the energy conversion efficiency in DSSCs. However, these structures are based on a complicated two-step process in which NWs are first prepared, followed by the growth of dendritic branches on the NW surfaces. To the best of our knowledge, there have been no reports of a one-step method for the preparation of such structures and their application in ssDSSCs, in which the effect of a 1D well-aligned structure is more obvious.

Here, we report hierarchical anatase pine tree-like TiO_2 nanotubes (PTT) arrays with NR branches directly grown on a transparent conducting oxide (TCO) substrate. The synthesis was based on a one-step hydrothermal method using potassium titanium oxide oxalate dehydrate (PTO), diethylene glycol (DEG), and water. The vertically aligned anatase TiO_2 NT arrays can enhance the charge transport while the NR branches provide a large surface area for a high dye loading. The resulting PTT arrays were characterized in detail using field-emission scanning electron microscopy (FE-SEM), energy-filtering transmission electron microscopy (EF-TEM), and X-ray diffraction (XRD). Three different types of PTT films were used as a photoelectrode in ssDSSCs with a solid polymerized ionic liquid (PIL).[5] Careful adjustment of the water/DEG ratio was utilized to systematically vary the TiO_2 structure and its effect on the cell performance. The ssDSSCs were characterized via current-voltage curves, the incident photon-to-electron conversion efficiency (IPCE), electrochemical impendence spectroscopy (EIS), and intensity-modulated photovoltage spectroscopy (IMVS)/intensity-modulated photocurrent spectroscopy (IMPS) measurements.

2. Results and Discussion

Hierarchical PTT arrays comprising a vertically-oriented long NT stem and short NR branches were directly grown on a fluorine-doped tin oxide (FTO) substrate via a one-step hydrothermal method. It is well known that a 1D well-aligned, nanostructural photoanode is effective in enhancing charge transport but the low surface area of such a structure limits the improvement of the current density.[29] Photoanodes derived from hierarchical PTT arrays can be one solution to simultaneously enhance the surface area and charge transport. Vertically aligned NTs can improve charge transport while the dendritic NR branches grown on the NTs can enhance the specific surface area, resulting in an improved charge collection efficiency.

Figure 1 shows SEM images of the cross-sectional view of PTT arrays at low and high magnifications, in which the NTs grew almost perpendicularly from the FTO substrate and are covered by a large number of NR branches. Preferential growth in the y-axial [001] direction over the x-axial [110] direction could be facilitated without pre-formation of a seed layer, which is commonly employed for the growth of NRs or NTs on FTO substrates.[29] The structure of the PTT arrays was strongly dependent on the water/DEG volume ratio. NTs with lengths of approximately 13.5 μm and NR branches with lengths and diameters of approximately 430 nm and 40 nm, respectively, were obtained at a water/DEG ratio of 1:4.7 ml (named PTT1, Figure 1a,b,c). Changing the water/DEG ratio to 1:3.4 (increasing water amount) promoted the growth of PTTs from a length of 13.5 to 16 μm (named PTT2), which represents a tremendous increment of about 19%. In this case, there was a slight decrease of the NR size with a length and diameter of 300 nm and 30 nm, respectively, as shown in Figure 1d,e,f. When using a larger amount of water, i.e., the water/DEG ratio = 1:2.6 (named PTT3, Figure 1g,h,i), the length of the NT stem further increased to approximately 19 μm, which is 19% and 40% larger than that of PPT2 and PPT1, respectively, and is one of highest ever reported for NTs.[29] The length and diameter of the NRs (PTT3) were approximately 230 nm and 20 nm, which are smaller than those of PPT1 or PPT2. Thus, it is concluded that the length of the NTs increased while the size of the NR branches decreased with increasing water content. A larger amount of water leads to more and stronger interactions between the water and PTO precursor through hydrogen bonding, which results in a decrease of the hydrolysis of the PTO precursor and eventually retards

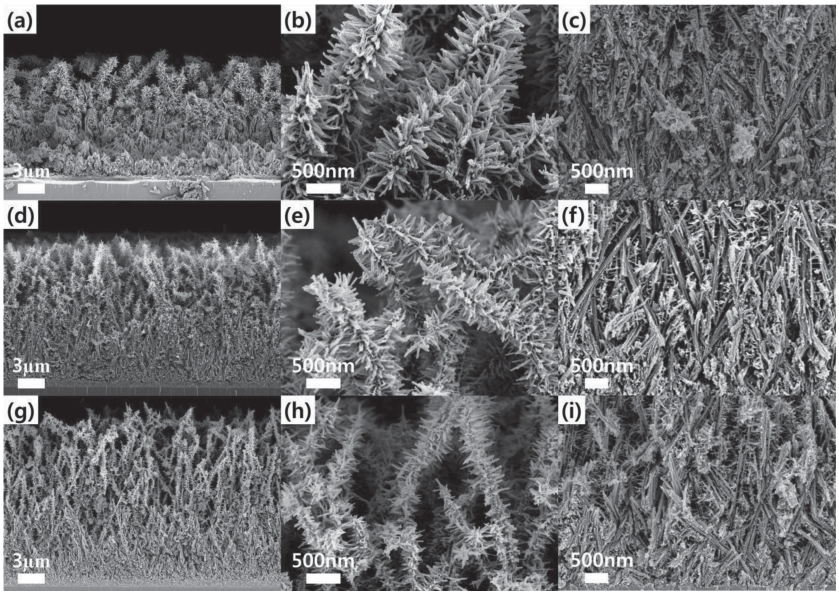

Figure 1. Cross-sectional FE-SEM images of the PTT arrays: (a) whole, (b) top, and (c) bottom regions of PTT1, (d) whole, (e) top, and (f) bottom regions of PTT2, and (g) whole, (h) top, and (i) bottom regions of PTT3.

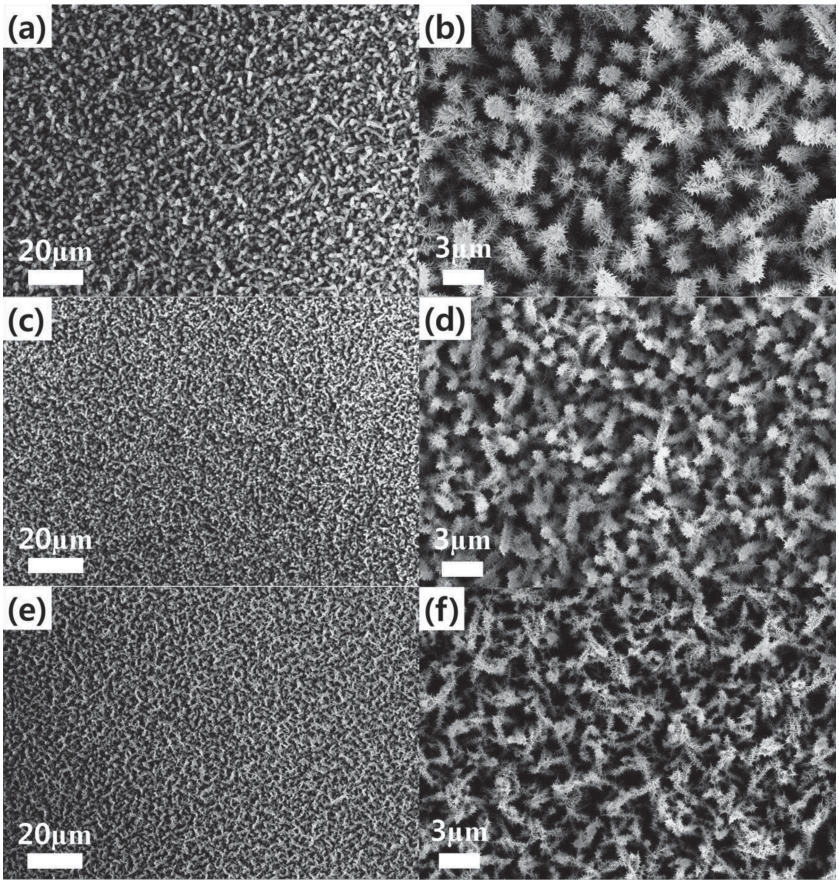

Figure 2. Top-down FE-SEM surface images of the PTT arrays at low and high magnifications: (a, b) PTT1, (c, d) PTT2, and (e, f) PTT3.

the nucleation and crystallization of TiO_2. This may help to produce a greater amount of TiO_2 sol participating in the nucleation of PTT, resulting in an increase of the PTT length.

The extremely long NTs and a large number of NRs in PTT3 are significant factors to increase not only the surface area but also the light scattering ability, resulting in an enhancement of the light harvesting efficiency of DSSCs. Although the length of the NR branches in PTT3 decreased, there was a significant increase in the number of NRs, which could offset the loss and thus, help to increase its specific surface area. As shown in the magnified SEM images, all of the PTT arrays exhibited an asymmetric structure in which more packed NT structures with a higher density are present in the bottom layer. The NTs consisted of multi-NWs with diameters of approximately 20 nm, which is more effective in improving the surface area and charge collection efficiency due to the well-developed structure with 1D growth on the FTO substrate. **Figure 2** shows SEM images of a top-down view of PTT arrays at low and high magnifications. The PTT arrays were arranged homogeneously and fully covered the FTO glasses without crack formation, indicating uniform growth anisotropy and large-scale processability.

The morphological and structural properties of the PTT arrays were further characterized by EF-TEM analysis. As shown in **Figure 3**, a large number of NR branches were directly grown on the NT stems in all of the PTTs. The NT structure is more advantageous than solidly packed NWs in DSSC applications because the sensitizer can be adsorbed outside as well as inside the NTs,[30] leading to a higher dye loading and current density. The wall thicknesses among the PTT arrays were not significantly different (approximately 25 nm). The magnified images reveal that PTT1, PTT2, and PTT3 contained a large number of NRs with lengths of 430, 300, and 230 nm and diameters of 40, 30, and 20 nm, respectively, which is consistent with the above SEM results. These 1D porous NT stems with NR branches would enhance the surface area and facilitate effective charge transport. Furthermore, they can be effective for facile pore infiltration of a solid electrolyte with a large molecular volume.

The crystal phase of TiO_2 is one of the important factors that directly affects the DSSC performance since it is related to the electron transfer properties and the amount of dye adsorption. The phase purity and structure of the PTT arrays were investigated by XRD analysis in the 2θ range of 15° to 80°, as shown in Figure S1. The sharp peaks at 25.4, 37.8, 48.1, 54.6, 55.3, 63.0, 69.7, and 75.4° correspond to the reflections from the (101), (004), (200), (105), (211), (204), (220), and (215) crystal planes of anatase TiO_2, respectively. A pure anatase phase of the PTT arrays is a very effective structure in DSSC applications due to its excellent electron transport, lower charge carrier recombination rate, and larger surface area.[31] The full width at half-maximum (FWHM) of the anatase (101) peak gradually increased in the order PTT1 < PTT2 < PTT3, indicating the reduced average crystalline size in the reverse order. The crystallite sizes of PTT1, PTT2, and PTT3 were determined from the Scherer equation to be 28.0, 23.3, and 20.0 nm, respectively.

The current density of DSSCs is closely related to the surface area of the TiO_2 photoanode, which in turn determines the amount of adsorbed dye. The amount of adsorbed dye was determined by adsorption–desorption measurements of the sensitizer on the PTT films and the results are summarized in **Table 1**. The dye loading amounts of photoanodes derived from PTT1, PTT2, and PTT3 were 83.5, 94.1, and 106.3 nmol/cm^2, respectively. The dye adsorption amount of PTT3 was the greatest among the PTT arrays, which is due to the extremely long NT stem and a large number of dendritic NR branches, as confirmed by the SEM and TEM analyses. The dye loading of the PTT3 film is approximately 28% greater than the amount of the PTT1 film, which appears to be low when compared to the 40% increase of the NT length. This is because an increase of the NT length accompanies a decrease of the length of the dendritic NR branches.

The current density-voltage (J-V) curves of the ssDSSCs fabricated with the PTT films and PIL as a photoanode and a solid electrolyte, respectively, were measured at 100 mW/cm^2,

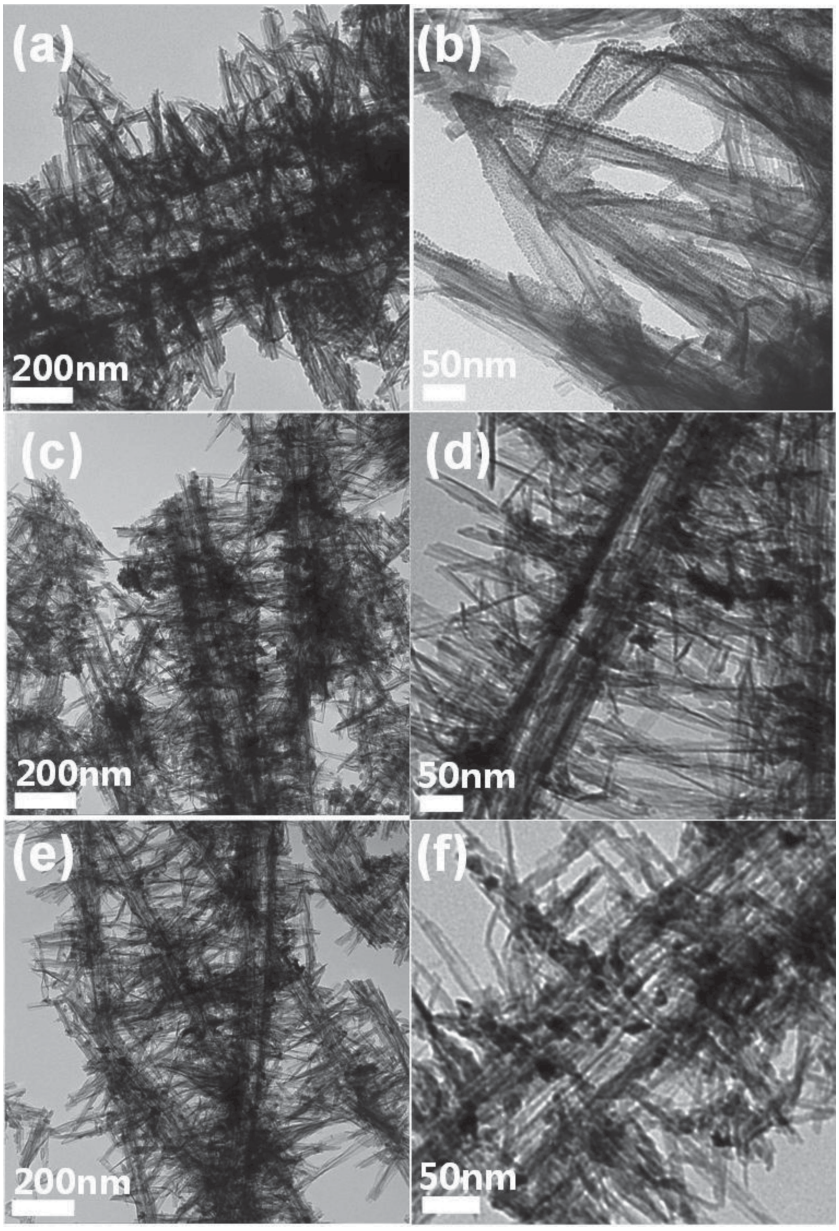

Figure 3. EF-TEM images of the PTT arrays at different magnifications: (a, b) PTT1, (c, d) PTT2, and (e, f) PTT3.

as shown in **Figure 4**(a). Poly((1-(4-ethenylphenyl)methyl)-3-butyl-imidazolium iodide) (PEBII) was synthesized via free radical polymerization as a PIL and utilized as a solid electrolyte for I_2-free ssDSSCs without using any additives.[5] The synthesized PEBII showed a high mobility and ionic conductivity (2.0×10^{-4} S/cm at 25 °C) due to facile ion transportation through the well-organized structure with π–π stacking interaction and a low glass transition temperature (~ –4 °C). The detailed photovoltaic properties including the open-circuit voltage (V_{oc}), short-circuit current density (J_{sc}), fill factor (FF), and energy conversion efficiency (η) are summarized in Table 1. The energy conversion efficiencies of all three PTT-based cells were much greater than that of the less organized TiO_2 cell (4.0%) fabricated using commercially available Dyesol paste 18NR-T. It should be noted that the efficiency of the less organized TiO_2 cell increased with increasing TiO_2 film thickness up to 8.5 μm, above which the efficiency gradually decreased due to ineffective pore infiltration of the large volume solid electrolyte, leading to poor electrode/electrolyte interfacial contact. The higher efficiencies of the PTT-based cells result from higher J_{sc} and FF values as the V_{oc} values among the cells are similar. The improved J_{sc} values result from the larger dye loading due to the larger surface area and very long NT structure. Also, the 1D well-developed organized structure allows for deep penetration of solid electrolyte to improve the electrode/electrolyte interfacial contact, leading to improved FF values. These results indicate the importance of a 1D well-aligned structure of a photoanode with large pore volumes in ssDSSCs, where deep penetration of solid electrolyte is most important and thus, the effect of an organized structure is obvious.

Table 1. Dye loading, photovoltaic properties, and internal resistances determined from J–V curves and EIS analysis at 100 mW/cm^2 of the ssDSSCs fabricated with the PTT arrays

	Thickness [μm]	Dye loading [nmol/cm^2]	V_{oc} [V]	J_{sc} [mA/cm^2]	FF	η [%]	R_s [Ω]	R_1 [Ω]	R_2 [Ω]
PTT1	13.5	83.5	0.75	13.8	0.63	6.6	9.7	8.9	39.5
PTT2	16.0	94.1	0.74	16.0	0.62	7.3	10.7	8.2	31.2
PTT3	19.0	106.3	0.74	17.7	0.62	8.0	10.2	8.1	25.8
Dyesol[a)]	8.5	83.2	0.73	11.0	0.50	4.0	–	–	–

[a)]Dyesol: commercially available Dyesol paste (18NR-T).

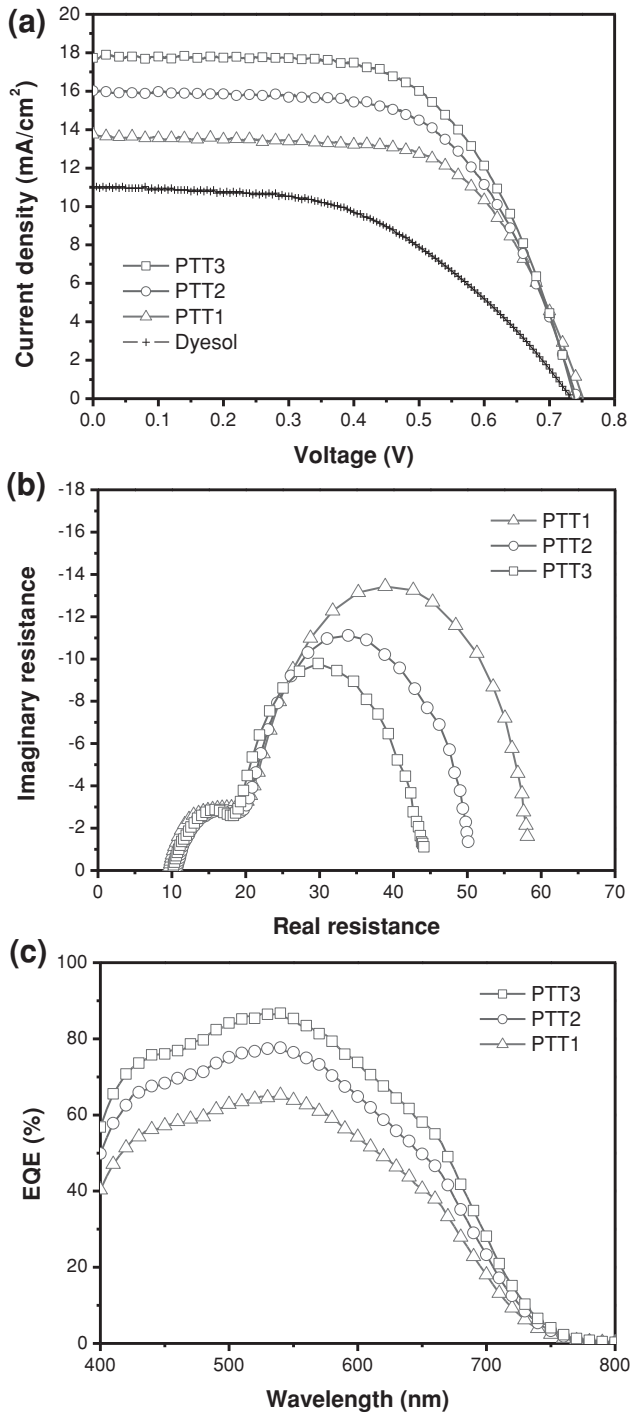

Figure 4. (a) J-V curves, (b) EIS data, and (c) IPCE spectra of ssDSSCs fabricated with the PTT arrays at 100 mW/cm^2.

These explanations are also supported by the result that the J_{sc} and FF values of PTT1 are much greater than those of Dyesol cell despite similar dye loading. The conversion efficiency of the ssDSSC derived from PTT3 reached 8.0% at 100 mW/cm^2, which is one of the highest values observed for N719-based ssDSSCs[3–17] and is two-fold greater than that of commercially available TiO_2. Also, the obtained cell efficiency was maintained at a nearly constant value for up to 200 h at room temperature. The efficiencies of liquid electrolyte-based DSSCs was only slightly higher than those of PEBII-based ssDSSCs, indicating more effectiveness of 1D nanotube structures in solid-state system.

The internal resistances in the ssDSSCs assembled with the PTT arrays were further characterized by EIS analysis. As shown in Figure 4b, two semicircles were achieved in the Nyquist plots of the ssDSSCs derived from the PTT arrays. The sheet resistance (R_s) is attributed to the ohmic resistance of the substrate. The first small semicircle (R_1), in the high-frequency region, is attributed to the charge transfer resistance at the counterelectrode/electrolyte interface. The second large semicircle (R_2), in the low-frequency region, is attributed to the charge transfer resistance at the photoelectrode/electrolyte interface.[32] These resistance values (R_s, R_1, and R_2) are summarized in Table 1. There was no large differences among the R_s values of all three devices, indicating a similar ohmic resistance of the substrate. However, the R_1 and R_2 values decreased from PTT1 to PTT3 due to the different electrode structures. In particular, the R_2 value of the PTT3-based cell was the smallest (25.8 Ω), indicating the greatest charge transfer properties at the photoelectrode/electrolyte interface.

The light scattering properties were also evaluated by measuring the IPCE spectra of the ssDSSCs based on PTT arrays as a function of wavelength, as shown in Figure 4c. The 65% external quantum efficiency (EQE) value of the PTT1 cell at around 530 nm improved to 77% for the PTT2 cell and further improved to 87% for the PTT3 cell. The tremendous increase of the IPCE value of the PTT3 cell is attributed to the larger dye loading amount, resulting in a higher short-circuit current density. The approximately 19 μm long NT arrays and a large number of NR branches provide a larger surface area and greater dye adsorption. The normalized IPCE curves in Figure S2 show that there was no significantly large difference of the quantum efficiencies of the PTT cells at longer wavelengths (>550 nm) but there was a tendency of the light scattering effect in the order of PTT3 > PTT2 > PTT1. Thus, it is concluded that the enhanced light scattering property of the PTT3 array contributed to the improvement of the energy conversion efficiency of the ssDSSC.

IMPS/IMVS measurements were performed to analyze the charge transport dynamics and charge recombination of the ssDSSCs derived from the PTT arrays. A diode laser with variable power and modulation control was used as the light source (635 nm) for these studies. The time delay in the IMPS measurement corresponds to the transport time of the injected electrons through the TiO_2 photoanode. The transport time can be estimated from the relationship $\tau_d = 1/2\pi f_{dmin}$, where f_{dmin} is the characteristic frequency at the minimum of the imaginary IMPS. The electron diffusion coefficient, D_n, was determined from the equation $D_n = d^2/(2.35\ \tau_d)$, where d is the thickness of the photoelectrode. The electron lifetime (τ_r) can be calculated from the expression $\tau_r = 1/2\pi f_{rmin}$, where f_{rmin} is the characteristic frequency minimum of the IMVS imaginary component.[33]

Figure 5a and b show the D_n and τ_r values obtained from the IMPS and IMVS measurements, respectively, plotted as a function of the current density. A higher electron diffusion

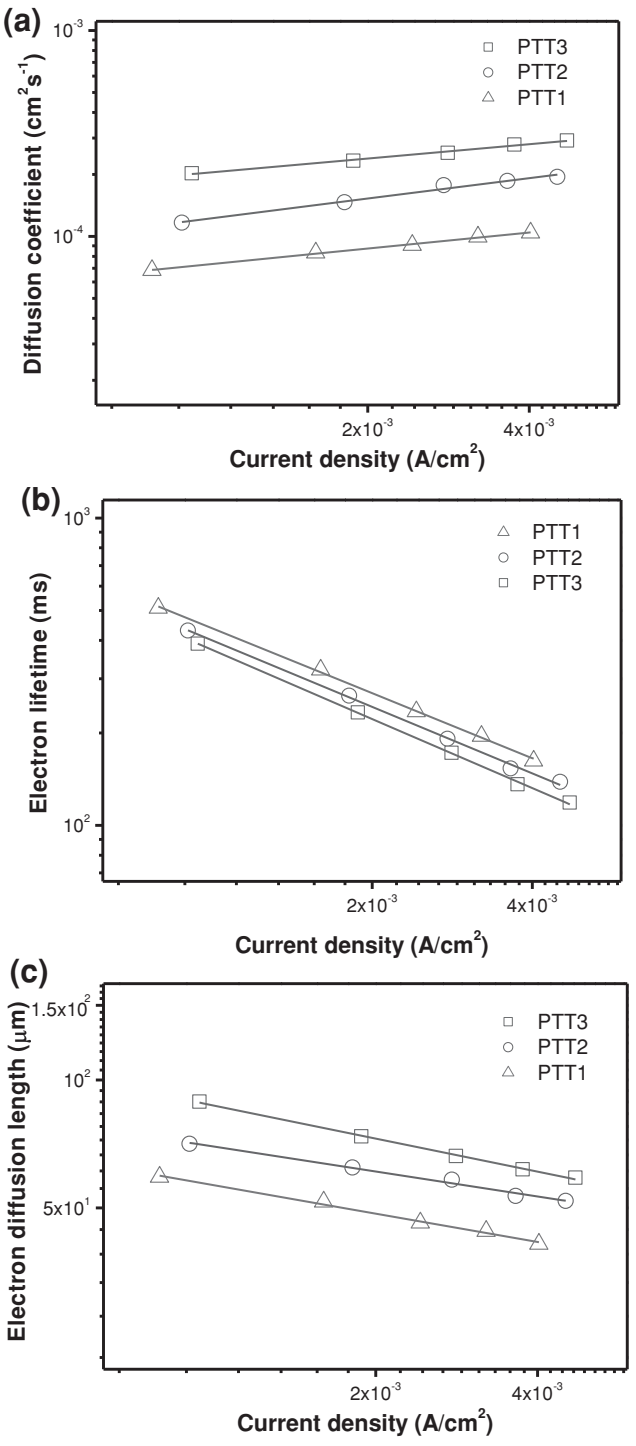

Figure 5. (a) Diffusion coefficient (D_n), (b) electron lifetime (τ_r), and (c) electron diffusion length (L_n) of ssDSSCs fabricated with the PTT arrays, as determined from IMPS/IMVS measurements.

coefficient was obtained from the PTT3 cell, indicating that the PTT3 arrays are more efficient in transporting electrons and thus, the travel time of photoinjected electrons from the excited dye to the electrode is short. A large number of short NR branches in PTT3 is efficient to shorten the electron transfer path and can easily concentrate electrons from dendritic NRs to NT stems. The fast electron transport rate improves the charge collection efficiency. On the other hand, the electron life time of the PTT3 cell was slightly shorter than those of the other cells. This is because the larger surface area of the PTT3 film provides more trapping sites and thus, leads to a larger charge recombination with I_3^- in the electrolyte.[34] As a result, a slight reduction of the V_{oc} (by 0.01 V) was observed in the cell derived from PTT3. The effective electron diffusion length (L_n) was obtained from $L_n = (D_n \cdot \tau_r)^{0.5}$, which is the average distance an injected electron can travel through the photoanode prior to undergoing recombination. A long electron diffusion length is an important element for DSSCs because only a small loss of injected charge occurs in the photoanodes with a longer electron diffusion length before it is collected. As shown in Figure 5c, the electron diffusion lengths of the cells derived from all of the PTT arrays were greater than 40 μm, which is much longer than the actual PTT length, demonstrating that the generated electrons can reach the electrode without losses and thus, a much thicker film can be fabricated without extra loss due to recombination.

3. Conclusion

Hierarchical anatase PTT arrays were prepared directly on a FTO substrate *via* a one-step hydrothermal method using PTO, DEG, and water. The resultant PTT consisted of long NT stems grafted with a large number of NR branches, which is an effective structure to improve the charge transport and specific surface area. The SEM analysis revealed that the PTT arrays possess asymmetric structures with the long NTs and short NR branches at the top layer and closely packed NWs or NTs at the bottom layer. Three different PTT arrays, PTT1, PTT2, and PTT3, were obtained by adjusting the water/DEG ratio. The diameter of the NTs and size of the NRs decreased with increasing water amount but the length of the PTT increased. This is because a larger amount of water leads to more and stronger interactions between water and the PTO precursor, which reduces the hydrolysis of PTO and retards the nucleation/crystallization of TiO_2, resulting in an increase of the PTT length. The largest length of the NTs (19 μm) was obtained for PTT3, which resulted in an enhanced surface area and a sufficient dye adsorption amount. The efficiencies of the PTT-based cells were always much greater than that of the less organized TiO_2 cell (4.0%) assembled using commercially available Dyesol paste 18NR-T, indicating the importance of a 1D well-aligned structure of the photoanode with large pore volumes in ssDSSCs. The conversion efficiency of the ssDSSC assembled with the PTT3 array reached 8.0% at 100 mW/cm^2, which is one of the highest values observed for N719-based ssDSSCs and is two-fold greater than that of commercially available TiO_2. The higher cell efficiency is attributed to the enhanced J_{sc} and FF values due to the well-aligned, interconnected structure with large pores and a high porosity, which is effective for solid electrolytes with large molecular volumes.

4. Experimental Section

Materials: Potassium titanium oxide oxalate dehydrate (PTO), diethylene glycol (DEG), titanium (IV) bis(ethylacetoacetato) diisopropoxide, and butanol were purchased from Aldrich. Ruthenium dye (535-bisTBA, N719) was purchased from Solaronix. Transparent conductive fluorine-doped tin oxide (FTO) conducting glass substrates (TEC8, 8 ohms/sq, 2.3 mm thick) were purchased from Pilkington, France. All solvents and chemicals were reagent grade and were used as received without further purification.

Synthesis of Hierarchical PTT Arrays: First, 0.73 g of PTO was dissolved in water and then, DEG was added to the solution. In order to control the morphology of the PTT arrays, water/DEG ratios of 1/4.7, 1/3.4 and 1/2.6 were used and the total volume of the mixed solutions was fixed at 40 ml. The mixed solutions were transferred to a FTO glass cleaned with isopropanol and chloroform placed against the wall of a Teflon-lined stainless steel autoclave. The hydrothermal reactions were carried out at 200 °C for 11 h. After the reaction, the as-prepared PTT samples were rinsed with water and ethanol several times, and then heated to 500 °C for 1 h in air to remove the residual DEG.

Fabrication of ssDSSCs: The ssDSSCs with an active area of 0.2 cm^2 were constructed by drop-casting the polymer electrolyte solution onto the photoanode and covering with the counter electrode, using a previously reported procedure.[5,16] First, the FTO glasses cleaned with isopropanol and chloroform were coated with a 2 wt% titanium (IV) bis(ethylacetoacetato)diisopropoxide solution in butanol as a blocking layer by spin coating followed by calcination at 450 °C for 30 min in air. Then, the PTT arrays were grown on the blocking layer-coated FTO glasses. As-prepared vertically aligned PTT arrays on the FTO were immersed in a 0.15 M $TiCl_4$ solution for 30 min at 70 °C. After washing with water and ethanol, the PTT films were heated in air at 450 °C for 30 min. The PTT films were sensitized by a 0.1 mM ruthenium dye (N719) in absolute ethanol at 50 °C for 2 h. The solid-state polymer electrolyte of poly((1-(4-ethenylphenyl)methyl)-3-butyl-imidazolium iodide) (PEBII, M_w = 15 000 g/mol)[5] was dropped on the dye-absorbed PTT photoanodes by two steps. First, a 2 wt% dilute PEBII solution in acetonitrile was dropped several times and then, a 10 wt% concentrated solution was dropped once. Pt-coated counter electrodes were prepared via spin coating of a 7 mM H_2PtCl_6 solution in isopropyl alcohol and calcination in air at 450 °C for 30 min. Then, the counter electrodes were assembled using the dye-sensitized photoanode. The cells were placed in a vacuum oven for a day to result in complete evaporation of the solvent and then sealed with epoxy resin.

Characterization: The morphology and structure of the PTTs arrays were observed using a field-emission scanning electron microscope (FE-SEM, SUPRA 55VP, Germany, Carl Zeiss) and an energy-filtering transmission electron microscope (EF-TEM, LIBRA 120). X-ray diffraction (XRD) measurements were carried out using a Rigaku RINT2000 wide-angle goniometer with a Cu cathode operated at 40 kV and 300 mA. The concentration of absorbed dye and reflectance spectra were measured using a UV-visible spectrophotometer (Shimadzu) in the range of 200 to 1100 nm. The photoelectrochemical performance characteristics including the short-circuit current (J_{sc}, mA/cm^2), open-circuit voltage (V_{oc}, V), fill factor (FF), and overall energy conversion efficiency (η) were measured using a Keithley Model 2400 and a 1000 W xenon lamp (Oriel, 91193). Six identical cells were assembled and characterized. The average estimated error was ± 3%. The light was homogeneous over up to an 8 × 8 in^2 area and its intensity was calibrated with a Si solar cell (Fraunhofer Institute for Solar Energy System, Mono-Si+KG filter, Certificate No. C-ISE269) at a sunlight intensity of 1 (100 mW/cm^2). This calibration was confirmed using a NREL-calibrated Si solar cell (PV Measurements Inc.). Intensity-modulated photovoltage spectroscopy (IMVS) and intensity-modulated photocurrent spectroscopy (IMPS) measurements were carried out using an electrochemical workstation equipped with a frequency response analyzer under a modulated green light-emitting diode (635 nm) driven by a source supply, which can provide both DC and AC illumination components. The frequency range was from 10 000 Hz to 0.01 Hz. Incident-photon-to-current efficiency (IPCE) spectra were obtained as a function of wavelength from 400 to 800 nm. The amount of adsorbed dye was determined by adsorption–desorption measurements of the sensitizer on the films. Dye desorption occurred after immersion of the TiO_2 film in a 10 mM solution of NaOH in an ethanol–water (1:1) mixture. The concentration of the desorbed dye solution was analyzed using a UV-visible spectrophotometer.

Supporting Information

Supporting Information is available from the Wiley Online Library or from the author.

Acknowledgements

This work was supported by the Active Polymer Center for Pattern Integration (R11–2007–050–00000–0), the Korea Center for Artificial Photosynthesis (KCAP) (2012M1A2A2671781), the Core Research Program (2012R1A2A2A02011268), and the Energy Efficiency & Resources of the Korea Institute of Energy Technology Evaluation and Planning (KETEP) (20122010100040).

Received: May 7, 2013
Revised: June 20, 2013
Published online: July 31, 2013

[1] a) B. O'Regan, M. Grätzel, *A Low-Cost, Nature* **1991**, *353*, 737–740; b) M. Grätzel *Nature* **2001**, *414*, 338–344.
[2] a) F. Huang, D. Chen, X. L. Zhang, R. A. Caruso, Y. C. Cheng, *Adv. Funct. Mater.* **2010**, *20*, 1301–1305; b) D. Chen, F. Huang, Y. B. Cheng, R. A. Caruso, *Adv. Mater.* **2009**, *21*, 2206–2210.
[3] a) S. Yanagida, Y. H. Yu, K. Manseki, *Acc. Chem. Res.* **2009**, *42*, 1827–1838; b) K. Manseki, W. Jarernboon, Y. Youhai, K. J. Jiang, K. Suzuki, N. Masaki, Y. Kim, J. B. Xia, S. Yanagida, *Chem. Commun.* **2011**, *47*, 3120–3122.
[4] a) S. Nejati, K. K. S. Lau, *Nano Lett.* **2011**, *11*, 419–423; b) C. Xu, J. Wu, U. V. Desai, D. Gao, *Nano Lett.* **2012**, *12*, 2420–2424.
[5] a) W. S. Chi, J. K. Koh, S. H. Ahn, J. S. Shin, H. Ahn, D. Y. Ryu, J. H. Kim, *Electrochem. Commun.* **2011**, *13*, 1349–1352; b) D. K. Roh, J. A. Seo, W. S. Chi, J. K. Koh, J. H. Kim, *J. Mater. Chem.* **2011**, *22*, 11079–11085; c) S. H. Ahn, W. S. Chi, D. J. Kim, S. Y. Heo, J. H. Kim, *Adv. Funct. Mater.* **2013**, DOI: 10.1002/adfm.201203851.
[6] H. Cao-Cen, J. Zhao, L. Qiu, D. Xu, Q. Li, X. Chen, F. Yan, *J. Mater. Chem.* **2012**, *22*, 12842–12850.
[7] Q. Li, J. Zhao, B. Sun, B. Lin, L. Qiu, Y. Zhang, X. Chen, J. Lu, F. Yan, *Adv. Mater.* **2012**, *24*, 945–950.
[8] a) C. P. Lee, P. Y. Chen, R. Vittal, K. C. Ho, *J. Mater. Chem.* **2010**, *20*, 2356–2361; b) C. Y. Hsu, Y. C. Chen, R. Y. Y. Lin, K. C. Ho, J. T. Lin, *Phys. Chem. Chem. Phys.* **2012**, *14*, 14099–14109.
[9] P. Docampo, S. Guldin, M. Stefik, P. Tiwana, M. C. Orilall, S. Huttner, H. Sai, U. Wiesner, U. Steiner, H. J. Snaith, *Adv. Funct. Mater.* **2010**, *20*, 1787–1796.
[10] S. Guldin, S. Huettner, P. Tiwana, M. C. Orilall, B. Uelguet, M. Stefik, P. Docampo, M. Kolle, G. Divitini, C. Ducati, S. A. T. Redfern, H. J. Snaith, U. Wiesner, D. Eder, U. Steiner, *Energy Env. Sci.* **2011**, *4*, 225–233.
[11] E. J. W. Crossland, M. Nedelcu, C. Ducati, S. Ludwigs, M. A. Hillmyer, U. Steiner, H. J. Snaith, *Nano Lett.* **2009**, *9*, 2813–2819.
[12] K. J. Jiang, K. Manseki, Y. H. Yu, N. Masaki, K. Suzuki, Y. L. Song, S. Yanagida, *Adv. Funct. Mater.* **2009**, *19*, 2481–2485.

[13] X. Z. Liu, W. Zhang, S. Uchida, L. P. Cai, B. Liu, S. Ramakrishna, *Adv. Mater.* **2010**, *22*, E150-E155.
[14] J. K. Koh, J. Kim, B. Kim, J. H. Kim, E. Kim, *Adv. Mater.* **2011**, *23*, 1641–1646.
[15] G. Q. Wang, L. A. Wang, S. P. Zhuo, S. B. Fang, Y. A. Lin, *Chem. Commun.* **2011**, *47*, 2700–2702.
[16] a) S. H. Ahn, W. S. Chi, J. T. Park, J. K. Koh, D. K. Roh, J. H. Kim, *Adv. Mater.* **2012**, *24*, 519–522; b) S. H. Ahn, J. H. Koh, Seo, J. A, J. H. Kim, *Chem. Commun.* **2010**, *46*, 1935–1937; c) D. K. Roh, J. T. Park, S. H. Ahn, H. Ahn, D. Y. Ryu, J. H. Kim, *Electrochim. Acta* **2010**, *55*, 4976–4981.
[17] a) Z. Lan, J. Wu, S. Hao, J. Lin, M. Huang, Y. Huang, *Energy Env. Sci.* **2009**, *2*, 524–528; b) Q. Li, X. Chen, J. Zhao, L. Qiu, Y. Zhang, B. Sun, F. Yan, *J. Mater. Chem.* **2012**, *22*, 6674–6679.
[18] I. Chung, B. Lee, J. He, R. P. H. Chang, M. G. Kanatzidis, *Nature*, **2012**, *485*, 486–489.
[19] a) M. M. Lee, J. Teuscher, T. Miyasaka, T. N. Murakami, H. J. Snaith *Science* **2012**, *338*, 643–647; b) H. S. Kim, C. R. Lee, J. H. Im, K. B. Lee, T. Moehl, A. Marchioro, S. J. Moon, R. Humphry-Baker, J. H. Yum, J. E. Moser, M. Gratzel, N. G. Park, *Sci. Rep.* **2012**, *2*, 591.
[20] K. Fan, W. Zhang, T. Peng, J. Chen, F. Yang, *J. Phys. Chem. C* **2011**, *115*, 17213–17219.
[21] a) X. Feng, K. Shankar, O. K. Varghese, M. Paulose, T. J. Latempa, C. A. Grimes, *Nano Lett.* **2008**, *8*, 3781–3786; b) M. Law, L. E. Greene, J. C. Johnson, R. Saykally, P. Yang, *Nat Mater* **2005**, *4*, 455–459.
[22] a) O. K. Varghese, M. Paulose, C. A. Grimes, *Nat. Nanotechnol.* **2009**, *4*, 592–597; b) M. H. Jung, M. J. Chu, M. G. Kang, *Chem. Commun.* **2012**, *48*, 5016–5018; c) M. Ye, D. Zheng, M. Lv, C. Chen, C. Lin, Z. Lin, *Adv. Mater.* **2013**, DOI:10.1002/adma.201205274.
[23] W. Yang, J. Li, Y. Wang, F. Zhu, W. Shi, F. Wan, D. Xu, *Chem. Commun.* **2011**, *47*, 1809–1811.
[24] F. Sauvage, D. Chen, P. Comte, F. Huang, L. P. Heiniger, Y. B. Cheng, R. A. Caruso, M. Graetzel, *ACS Nano* **2010**, *4*, 4420–4425.
[25] B. Liu, A. Khare, E. S. Aydil, *Chem. Commun.* **2012**, *48*, 8565–8567
[26] T. Krishnamoorthy, V. Thavasi, G. M. Subodh, S. Ramakrishna, *Energy Env. Sci.* **2011**, *4*, 2807–2812.
[27] J. Y. Kim, K. J. Lee, S. H. Kang, J. Shin, Y. E. Sung, *J. Phys. Chem. C* **2011**, *115*, 19979–19985.
[28] J. K. Koh, J. H. Koh, S. H. Ahn, J. H. Kim, Y. S. Kang, *Electrochim. Acta* **2010**, *55*, 2567–2574.
[29] a) F. Shao, J. Sun, L. Gao, S. Yang, J. Luo, *J. Mater. Chem.* **2012**, *22*, 6824–6830; b) J. Y. Liao, B. X. Lei, H. Y. Chen, D. B. Kuang, C. Y. Su, *Energy Env. Sci.* **2012**, *5*, 5750–5757; c) M. Ye, D. Zheng, M. Lv, C. Chen, C. Lin, Z. Lin, *Adv. Mater.* **2013**, DOI:10.1002/adma.201205274.
[30] D. K. Roh, R. Patel, S. H. Ahn, D. J. Kim, J. H. Kim, *Nanoscale* **2011**, *3*, 4162–4169.
[31] N. G. Park, J. van de Lagemaat, A. J. Frank, *J. Phys. Chem. B* **2000**, *104*, 8989–8994.
[32] M. Wu, X. Lin, T. Wang, J. Qiu, T. Ma, *Energy Env. Sci.* **2011**, *4*, 2308–2315.
[33] a) S. Wang, X. Zhang, G. Zhou, Z. S. Wang, *Phys. Chem. Chem. Phys.* **2012**, *14*, 816–822; b) W. Chen, Y. Qiu, S. Yang, *Phys. Chem. Chem. Phys.* **2010**, *12*, 9494–9501.
[34] Y. C. Qiu, W. Chen, S. H. Yang, *Angew. Chem.-Int. Ed.* **2010**, *49*, 3675–3679.